Title
Myelin degeneration and diminished myelin renewal contribute to age-related deficits in memory

Permalink
https://escholarship.org/uc/item/8fk9h5d5

Journal
Nature Neuroscience, 23(4)

ISSN
1097-6256

Authors
Wang, Fei
Ren, Shu-Yu
Chen, Jing-Fei
et al.

Publication Date
2020-04-01

DOI
10.1038/s41593-020-0588-8

Peer reviewed

Myelin degeneration and diminished myelin renewal contribute to age-related deficits in memory

Fei Wang[1,5], **Shu-Yu Ren**[1,5], **Jing-Fei Chen**[1], **Kun Liu**[1], **Rui-Xue Li**[1], **Zhi-Fang Li**[1,2], **Bo Hu**[3], **Jian-Qin Niu**[1], **Lan Xiao**[1], **Jonah R. Chan**[4,*], **Feng Mei**[1,*]

[1]Department of Histology and Embryology, Chongqing Key Laboratory of Neurobiology, Brain and Intelligence Research Key Laboratory of Chongqing Education Commission, Third Military Medical University, Chongqing, China.

[2]Department of Neurology, Fifth Medical Center of Chinese PLA General Hospital, Beijing, China.

[3]Department of Physiology, Third Military Medical University, Chongqing, China.

[4]UCSF Weill Institute for Neurosciences, Department of Neurology, University of California at San Francisco, San Francisco, CA, USA.

[5]These authors contributed equally: Fei Wang, Shu-Yu Ren.

Abstract

Cognitive decline remains an unaddressed problem for the elderly. We show that myelination is highly active in young mice and greatly inhibited in aged mice, coinciding with spatial memory deficits. Inhibiting myelination by deletion of Olig2 in oligodendrocyte precursor cells impairs spatial memory in young mice, while enhancing myelination by deleting the muscarinic acetylcholine receptor 1 in oligodendrocyte precursor cells, or promoting oligodendroglial differentiation and myelination via clemastine treatment, rescues spatial memory decline during aging.

Preventing age-related cognitive decline represents an unmet need for the elderly[1]. Multiple lines of magnetic resonance imaging evidence have identified abnormalities in the white matter of aged human brains[2]. Recent studies have revealed that myelin remodeling persists

in the adult mouse CNS[3–6]. Myelination is important for motor learning, and also adaptively responds to sensory cues[3,7,8]. Myelin remodeling in the adult CNS primarily results from myelin degeneration and addition of adult-born oligodendrocytes and myelin sheaths, which are derived from the differentiation of oligodendrocyte precursor cells (OPCs)[3,4,9,10].

To characterize myelin dynamics during aging, we examined myelin basic protein (MBP) expression and CC1-positive mature oligodendrocytes in 4-, 13- and 18-month-old brains (Extended Data Fig. 1a,b). In layers I–III of the motor cortex (where myelin is less dense), MBP intensity and oligodendrocyte number were significantly increased from 4 months to 13 months and then decreased by 35% at 18 months, while the Cspg4 (NG2)-positive OPC numbers were unaltered (Extended Data Fig. 1). We used the *Cspg4-CreERt;Mapt(tau)-mGFP* mice to label newly formed myelin sheaths in the mature adult (4–6 months) and middle-aged (13–17 months) mice (Extended Data Fig. 2)[4,11,12]. The mGFP-positive oligodendrocytes and myelin sheaths were visualized throughout the brain; for example, cortex, corpus callosum, hippocampus and striatum (Fig. 1a). Noticeably, numerous mGFP-positive myelin sheaths were seen in the 6- or 8-month-old corpus callosum, 2 months after recombination (Fig. 1b,c). By contrast, mGFP-positive myelin sheaths were sparsely distributed in the 18- and 22-month-old corpus callosum, even 5 months after recombination (Fig. 1b,c), indicating that myelination decreases in an age-dependent manner and that there is a steep decline after 13 months of age. Since the extent of newly generated myelin sheaths is relatively low in the aging brain, it is possible that the decrease in myelin in the 18-month-old cortex is due to both myelin degeneration and inefficient myelin renewal. To assess the stability of pre-existing myelin sheaths in mature adult mice, we crossed the *PLP-CreERt* line to the *mTomato/mGFP (mT/mG)* line and induced recombination at 3 months. The mGFP expression colocalized with MBP-positive myelin sheaths 1 month after recombination (Extended Data Fig. 3a). We found that the mGFP-positive areas were significantly decreased by ~10% in layers I–III of the 3 + 10-month cortex (Extended Data Fig. 3b), suggesting that the majority of myelin sheaths that are generated before 3 months are stable over the subsequent 10 months.

We next crossed the *Cspg4-CreERt* line to the *mT/mG* line to examine recombination efficiency in OPCs (Extended Data Fig. 4). More than 90% of Cspg4-positive OPCs expressed mGFP 10 d after tamoxifen treatment in both the 4-month-old and 13-month old mice (Extended Data Fig. 4), indicating similar recombination efficiency at different ages. On differentiation, mGFP-positive cells expressed MBP and CC1 (Extended Data Fig. 5a–c). Pericytes also expressed mGFP and were closely associated with mTomato-positive blood vessels (Extended Data Fig. 5a)[3,5]. To clearly view newly generated oligodendrocytes and myelin sheaths, we subtracted the pericytes, and pseudo-colored the mGFP OPCs in red (Cspg4-positive) (Extended Data Fig. 6a). Consistently, far fewer myelin sheaths were generated in the 13-month-old corpus callosum compared with the 4- and 8-month-old brains 10 d after recombination, despite similar OPC densities (Extended Data Fig. 6b). Next, 4- and 13-month-old mice were challenged with the water maze task (Fig. 1d–f) and a deficit in learning and memory was detected in the aging mice (Fig. 1d–f). As hippocampus is crucial for memory storage, we examined myelination in the hippocampal CA1 region (Fig. 1g). Our results indicate that newly formed myelin sheaths were greatly decreased in the CA1 region and neighboring corpus callosum in the middle-aged mice, with no change

in OPC density (Fig. 1h,i). Consistently, MBP expression was also decreased in the 18-month-old hippocampus compared with 13-month-old brains (Extended Data Fig. 7). Together, these results demonstrate an age-related decline in myelination coinciding with spatial learning and memory deficits.

Since the memory deficit emerges concomitantly with decreased myelination in the aging process, we asked whether active myelination is required for spatial memory. To specifically manipulate myelination in mature adult mice, we crossed the *Cspg4-CreERt;Mapt-mGFP* line to the *Olig2* floxed mouse line (*Olig2^fl/fl*) to delete Olig2 in adult OPCs and also visualize newly generated myelin in 4-month-old mice. Given that Olig2 is an important transcription factor in regulating the differentiation of OPCs[13], conditional deletion of Olig2 in adult OPCs resulted in a significant decrease in mGFP-positive oligodendrocytes and myelin sheaths 4 weeks after recombination in the corpus callosum, cortex and hippocampus of the Olig2 conditional knockout (cKO) brains (*Cspg4-CreERt;Olig2^fl/fl;Mapt-mGFP*) when compared with the heterozygote littermates (*Cspg4-CreERt; Olig2^fl/+;Mapt-mGFP*) (Fig. 2a–e). The Olig2 deletion did not significantly alter the number of mature oligodendrocytes (CC1-positive), OPCs (Cspg4-positive) or microglia (Iba1-positive) in the brains (Extended Data Fig. 8a). After 3 d of training in the water maze, the Olig2 cKO mice exhibited a significantly lower frequency of crossing in the target sector (Fig. 2f–i). Consistently, the distance traveled in the platform quadrant and the time in the target sector were also significantly decreased in the Olig2 cKO mice compared with the littermate controls (Fig. 2f–i). The *Olig2* heterozygotes displayed similar capacity in the water maze test compared with wild-type controls (*Olig2^+/+*) (Extended Data Fig. 8b). These results demonstrate that active myelination is required for spatial memory.

We next asked whether enhancing oligodendroglial differentiation and myelination represents a means to improve memory function in older mice. This task is challenging as oligodendroglial differentiation and myelination are greatly inhibited in the aged CNS by multiple inhibitory mechanisms, probably due to intrinsic (for example, epigenetic modifications) and extrinsic (for example, myelin debris) factors[14–16]. Our previous work implicates the muscarinic acetylcholine receptor 1 (Chrm1) as a potent negative regulator of oligodendroglial differentiation and myelination[11,12]. We crossed the *Chrm1* floxed line with the *Cspg4-CreERt;Mapt-mGFP* mice (*Cspg4-CreERt;Chrm1^fl/fl;Mapt-mGFP*). Recombination was induced by administration of tamoxifen at 13 months, when myelin loss was initially detected and myelin renewal was greatly diminished (Fig. 3a). Surprisingly, the Chrm1 deletion in OPCs resulted in a ~5-fold increase in mGFP-myelin expression in the corpus callosum, cortex and hippocampus at 18 months compared with age-matched wild types (*Cspg4-CreERt;Mapt-mGFP*) without affecting vascular density (CD31-positive) and microglia (Iba1-positive) (Fig. 3a–c and Extended Data Fig. 9a–d), indicating that the deletion of Chrm1 in OPCs can enhance differentiation and myelination even in the aging CNS. In keeping with the suggestion that age-related synaptic loss is an important indicator of declining hippocampal function[17], we found that the densities of synaptic puncta (both synapsin1 and vGlut1) were remarkably increased in the CA1 region of the Chrm1 cKO hippocampus compared with the wild types (Fig. 3d,e). The Chrm1 cKO mice displayed significant improvement in water maze task performance, showing increased frequency of target sector crossing, and greater time and distance traveled in the platform quadrant (Fig.

3f–i). Finally, we treated 12-month-old mice with clemastine at 10 mg kg^{-1} per day for 4 months (Fig. 3j)[18]. Clemastine treatment not only significantly enhanced myelination, as revealed in the *Cspg4-CreERt;mT/mG* mice (Fig. 3k), but also preserved spatial memory capacity in the water maze test (Fig. 3l). Collectively, our data indicate that rejuvenating myelination can rescue synaptic loss in the hippocampus and improve memory function in aging mice.

Magnetic resonance imaging evidence suggests that white matter volume in aged human brains is prominently decreased[2]. Our results suggest that both myelin degeneration and diminished renewal may contribute to the age-related decrease of white matter volume. Additionally, our findings indicate that spatial memory function also requires dynamic myelination in mature adult brains. Thus, the decline in memory can be attributed, at least in part, to diminished myelination in aging mice. It remains unclear from current data whether the myelin degeneration contributes to memory decline. It is plausible that the loss of myelin may disrupt or slow down the conduction of neuronal signals in the aged brains.

OPCs populate the aged CNS and maintain their potential to differentiate and myelinate[4,19]. Here, we find that enhancing endogenous myelination by Chrm1 deletion improves spatial memory function in old mice. As a proof of concept, we have shown that clemastine treatment reverses age-related memory decline. Although underlying mechanisms remain unclear, it is possible that newly formed myelin sheaths may preserve axonal integrity and functions[20]. In support of this notion, our recent data have shown that enhancing endogenous myelination in hypoxic neonatal mice improves neuronal function in adulthood[11]. It is important to note that, while these studies seemingly suggest that the effects on behavior are likely due to myelination, it is possible that the differentiation of mature oligodendrocytes is also responsible. While it is currently difficult to uncouple differentiation effects from a causative role for myelination in the profound behavioral effects observed, our findings lay the groundwork for future mechanistic studies and illustrate that oligodendrocytes play an important role in preserving brain function.

Methods

Animals.

All strains of mice were on a C57BL/6 background. The C57BL/6 mice of different ages for Morris water maze and drug treatment were purchased from the Laboratory Animal Center of the Third Military Medical University. The reporter gene mice, *mT/mG* (The Jackson Laboratory, catalog no. 007676) and *Mapt-mGFP (Tau-mGFP)* (catalog no. 021162), have been described previously[3–5,11]. They were crossed with *Cspg4-CreERt* (The Jackson Laboratory, catalog no. 008538) to initiate recombination in OPCs. The *mT/mG* line was also crossed with the *PLP-CreERt* line (The Jackson Laboratory, catalog no. 005795) to generate the *PLP-CreERt;mT/ mG* mice. The *Olig2* floxed line was crossed with the *Cspg4-CreERt;Mapt-mGFP* line to obtain *Cspg4-CreERt;Mapt-mGFP;Olig2$^{fl/fl}$* mice and littermates (*Cspg4-CreERt2;Mapt-mGFP;Olig2$^{fl/+}$*). The *Chrm1* floxed line was crossed with the *Cspg4-CreERt;Mapt-mGFP* line to obtain *Cspg4-CreERt;Mapt-mGFP;Chrm1$^{fl/fl}$* mice. Genotypes of all mice were determined using a PCR analysis of tail genomic DNA with appropriate primers. Male and female mice were used for all experiments without bias.

All animals were fed or bred in accordance with an approved protocol from the Laboratory Animal Welfare and Ethics Committee of the Third Military Medical University.

Administration of tamoxifen.

To induce Cre recombination, tamoxifen (Sigma-Aldrich, catalog no. T5648) was dissolved in sunflower oil at a concentration of 30 mg ml^{-1} and administered to the adult mice at 100 mg kg^{-1} for 4 consecutive days by oral gavage.

Drug treatment.

The 12-month-old mice were treated with clemastine (SelleckChem, catalog no. S1847) or an equivalent volume of vehicle. Clemastine was dissolved into drinking water and the mice were proximately dosed at 10 mg kg^{-1} per day for 4 months. Drug treatment was discontinued 1 week before the behavioral test.

Tissue processing and stereology.

Mice were deeply anesthetized with 1% pentobarbital and transcardially perfused with 4% paraformaldehyde in 0.1 M phosphate buffer after an initial flush with warm 0.01 M PBS. Brains were collected and postfixed in 4% paraformaldehyde in 0.1 M phosphate buffer overnight, then these tissues were dehydrated in 30% sucrose in 0.01 M PBS until submerging to the bottom. Brains were embedded in optimal cutting temperature compound (O.C.T. Compound, SAKURA, 4583) and then sliced coronally at 20-μm equidistant intervals using a cryostat microtome (MS 1850, Leica). Brain sections were collected from the tissues, including corpus callosum and hippocampus (from Bregma 1.1 mm to Bregma −2.70 mm in adult mice), in 24-well plates. To sample in a systematic, random manner, a set of 5–8 sections were sampled from the consecutive sections of each brain. In practice, the first one was randomly sampled from the first 20 consecutive sections and the following one was collected every other 20 consecutive sections.

Immunofluorescence staining.

For immunofluorescence staining, free floating sections were blocked with 5% BSA and 0.2% Triton-X 100 for 2 h at room temperature, and then sequentially incubated with primary antibodies overnight at 4 °C and the fluorescent-dye-conjugated secondary antibodies for 2 h at room temperature. Primary antibodies include: rabbit anti-Cspg4 (1:500; Millipore, catalog no. MAB5320), rabbit anti-NF200 (1:1,000; Sigma-Aldrich, catalog no. N4142), goat anti-MBP (1:200; Santa Cruz, catalog no. sc-13914), rat anti-MBP (1:500; Millipore, catalog no. MAB386), mouse anti-CC1 (1:500; Calbiochem, catalog no. OP80), guinea pig anti-vGlut1 (1:2,000; Synaptic Systems, catalog no. 135304), rat anti-CD31(1:200; BD Biosciences, catalog no. 553370), rabbit anti-Iba1(1:200; Wako, catalog no. 019–19741), rabbit anti-synapsin-1 (1:1,000; CST, catalog no. 5297) and chicken anti-MAP2 (1:2,000; EMD Millipore, catalog no. AB5543). Appropriate Alexa Fluor-conjugated secondary antibodies include donkey anti-mouse, donkey anti-rabbit, donkey anti-goat, goat anti-guinea and goat anti-chicken (1:1,000; Life Technologies). Sections were counterstained with DAPI.

Morris water maze.

The test was conducted according to a described protocol[21]. Briefly, the water maze was divided into four quadrants. In the acquisition phase, all mice were tested four times daily for 3–5 consecutive days, and the animals started from different quadrants every day to find the hidden platform at a fixed location. After the acquisition phase, the platform was removed and time spent in the platform-located quadrant, distance traveled in the platform quadrant or times crossing the platform area was measured to test long-term spatial memory. All tests were performed from 12:00 to 18:00. Investigators were blinded for genotype and mice were handled gently to avoid stress in the experiment.

Image acquisition and quantification.

Fluorescent images were captured using a confocal laser-scanning microscope (Olympus, FV 3000) with excitation wavelengths appropriate for Alexa Fluor 488 (488 nm), 596 (568 nm) or 647 (628 nm) or DAPI (380 nm). For the statistical analysis, the area of corpus callosum, hippocampus (CA1 region) or motor cortex was acquired from each sample for quantification. Detection and quantification were performed using Image-Pro Plus 5 (Media Cybernetics).

Synaptic puncta quantification.

At least three representative fields (oil, ×63) were randomly acquired from the CA1 area of the hippocampus by using a confocal laser-scanning microscope (Olympus, FV1000) to quantify synaptic puncta (synapsin1 and vGlut1) density. All of the images were acquired from the same Z positive using standardized imaging parameters throughout. To separate puncta from background, the threshold was set to at least two times the background intensity. Puncta were defined by distinct intensity peaks above the threshold.

Microglial morphology assay.

The entire microglia were scanned and imaged on Z-stacks at an interval 0.74 μm by using a confocal laser-scanning microscope (Olympus, FV1000) with a ×63 objective (oil, numerical aperture 1.3). All of the parameters were consistent throughout all experiments. Three-dimensional surface rendering of microglial images was created using Avizo software (2019.1, Thermo Fisher).

Statistical analysis.

No statistical methods were used to predetermine sample sizes, but our sample sizes are similar to those reported in previous publications[3,5]. Mice were randomly assigned to experimental time points or groups, and no animals or data points were excluded from analyses. Investigators were blinded to group allocation during data collection and analysis. All graph data are presented as the mean ± s.e.m. Points represent individual animals. Data distribution was assumed to be normal and this was not formally tested. Data of the acquisition phase in the Morris water maze were analyzed by separate repeated-measures two-way analysis of variance (ANOVA). For the other data, statistical difference between groups was determined using two-tailed unpaired t-test or one-way ANOVA followed by post hoc Tukey test for the normally distributed data. Nonparametric Mann–Whitney test

was used when the raw data displayed an abnormal distribution. The statistical methods, exact n values, significant and nonsignificant P values and degrees of freedom are described in the figure legends. Significance was reported as $*P < 0.05$, $**P < 0.01$ or $***P < 0.001$.
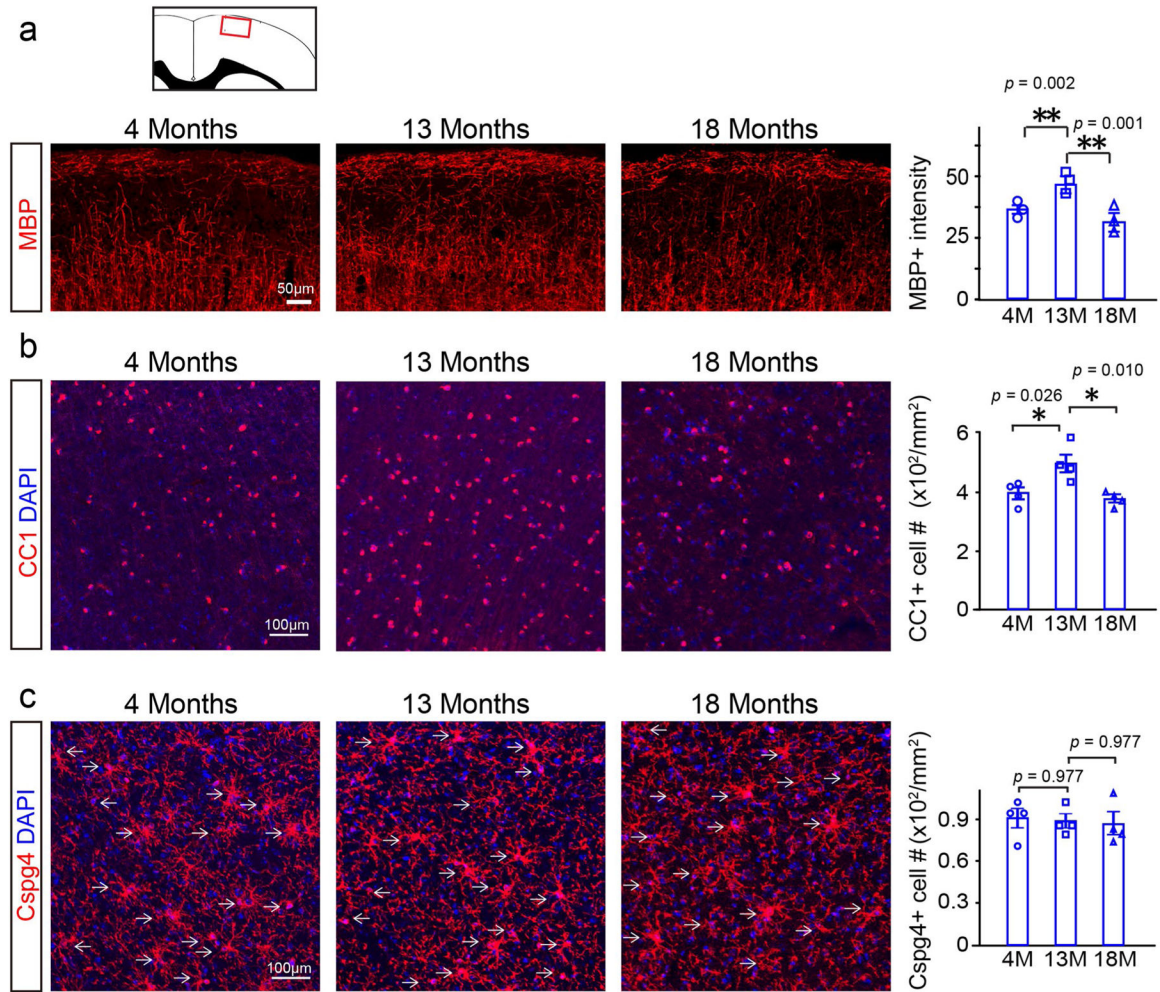
Reporting Summary.

Further information on research design is available in the Nature Research Reporting Summary linked to this article.

Data availability

Data from this study are available from the corresponding author upon reasonable request.

Extended Data

Extended Data Fig. 1 |. age-related myelin and oligodendrocyte loss.
a, Representative images and quantification of mean MBP intensity, n = 3 biologically independent mice, one-way ANOVA followed by post hoc Tukey test was used ($F_{(2,6)}$ = 31.35, p < 0.001, TUKEY (4 M versus 13 M): p = 0.002, TUKEY (13 M versus 18 M): p = 0.001). Scale bar = 50 μm; **b**, Representative images and quantification of CC1 positive cells, n = 4 biologically independent mice, one-way ANOVA followed by post hoc Tukey test was used ($F_{(2,9)}$ = 8.466, p = 0.009, TUKEY (4 M versus 13 M): p = 0.026, TUKEY (13 M versus 18 M): p = 0.010), scale bar = 100 μm; **c**, Representative images and quantification of Cspg4 positive cells, n = 4 biologically independent mice, one-way ANOVA followed by post hoc Tukey test was used ($F_{(2,9)}$ = 0.086, p = 0.919), scale bar = 100 μm. Points represented individual animals. Error bars represent mean ± s.e.m. *p < 0.05, **p < 0.01.
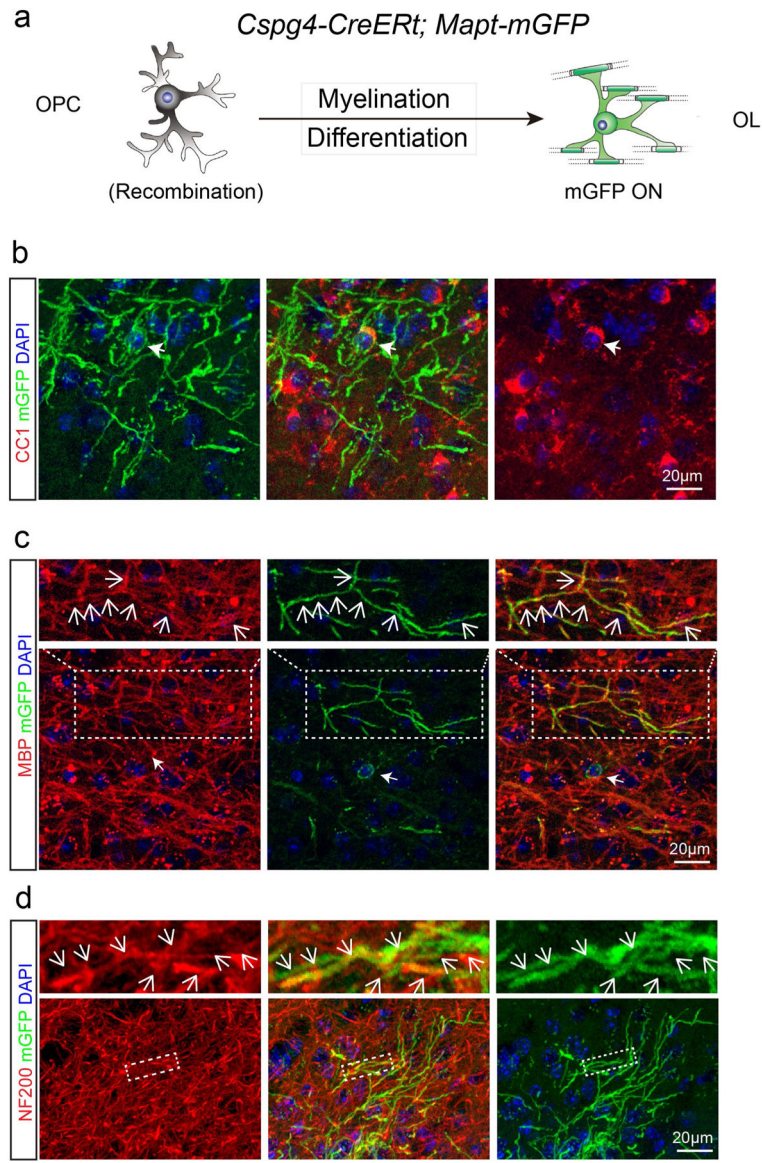
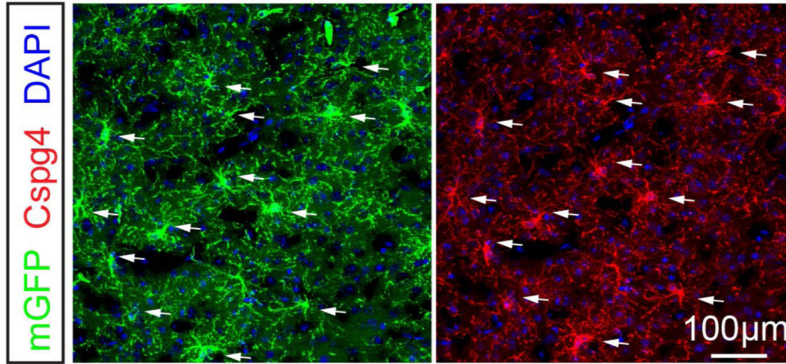**Extended Data Fig. 2 |. identification of mGFP positive cells.**
a, Schematic illustration showing mGFP expression in the *Cspg4-CreERt; Mapt-mGFP* mice; **b–d**, Immunostaining indicates that mGFP positive cell bodies are CC1 positive (**b**) and mGFP positive segments are co-localized with MBP (**c**) and associated with NF200 positive axons (**d**). These experiments were repeated 3 times independently with similar results, scale bar = 20 μm.
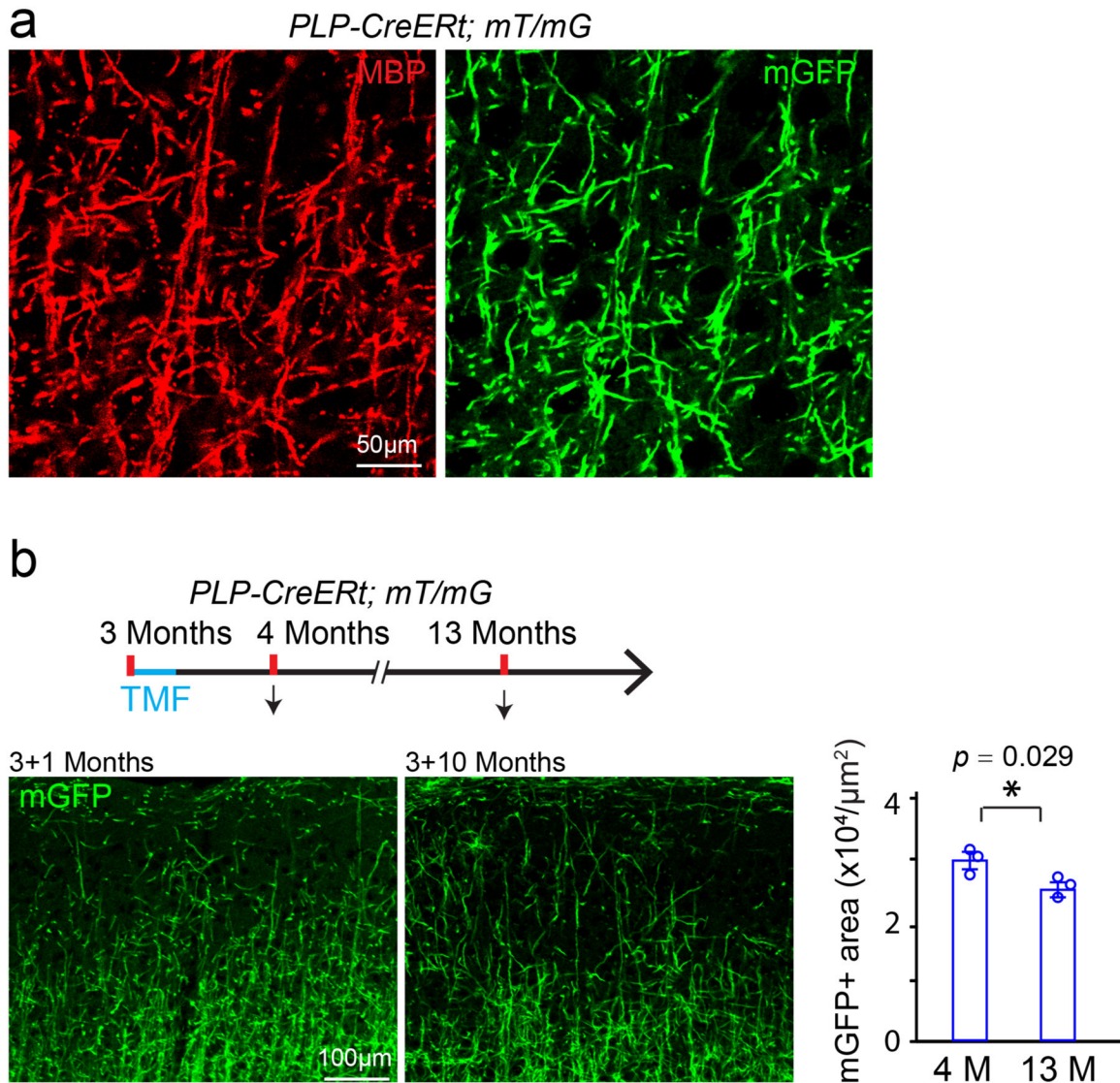
Extended Data Fig. 3 |. Stability of myelin sheaths in *PLP-CreERt; mT/mG* mice.
a, Representative image showing mGFP positive areas are co-localized with MBP positive myelin sheaths in the cortex of *PLP-CreERt; mT/mG* mice, 10 days after recombination at 3 months. These experiments were repeated 3 times independently with similar results. Scale bar = 50 μm; **b**, Schematic diagram displaying the time course of tamoxifen induction and histology, and representative images and quantification of the mGFP positive areas in the layers I-III of the cortex 1 or 10 months after recombination at 3 months. These experiments were repeated 3 times with similar results, n = 3 biologically independent mice for each group, two-tailed unpaired t test was used ($t_{(4)}$ = 3.327, p = 0.0292). Scale bar = 100 μm. Points represented individual animals. Error bars represent mean ± s.e.m. *p < 0.05.
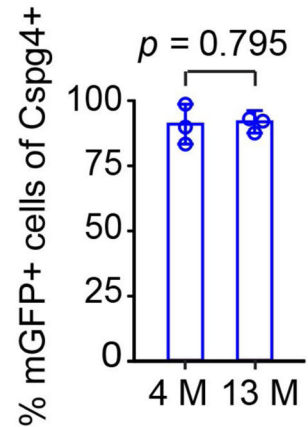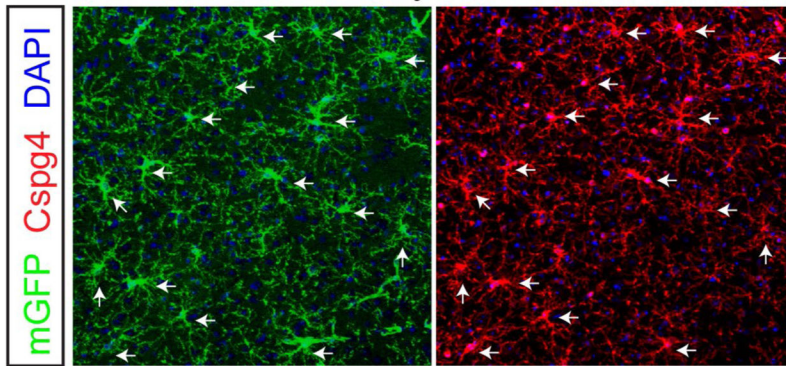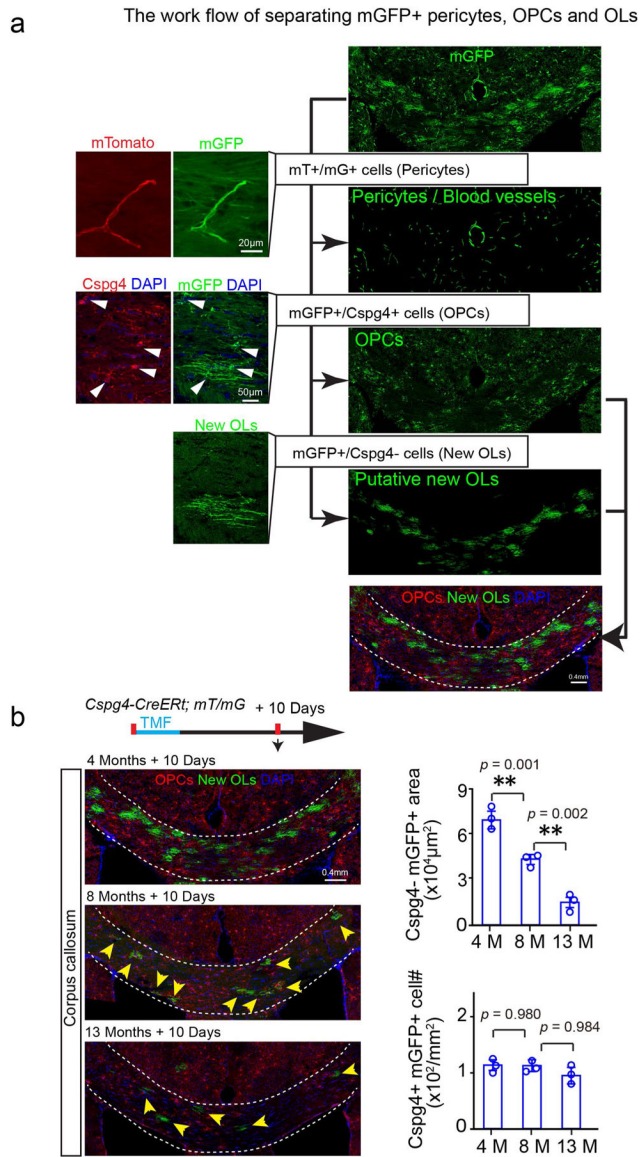
Extended Data Fig. 4 |. Recombination efficiency in 4- and 13-month old *Cspg4-CreERt; mT/mG* mice.
Representative images and quantification of the percentage of mGFP (green) positive cells in the Cspg4 (red) positive cells (OPCs) by immunostaining, 10 days after 4 consecutive days of tamoxifen treatment. Arrows indicating Cspg4/mGFP double positive cells, n = 3 biologically independent mice for each group, two-tailed unpaired t test was used ($t_{(4)}$ = 0.2774, p = 0.7953), scale bar = 100 μm. Points represented individual animals. Error bars represent mean ± s.e.m.
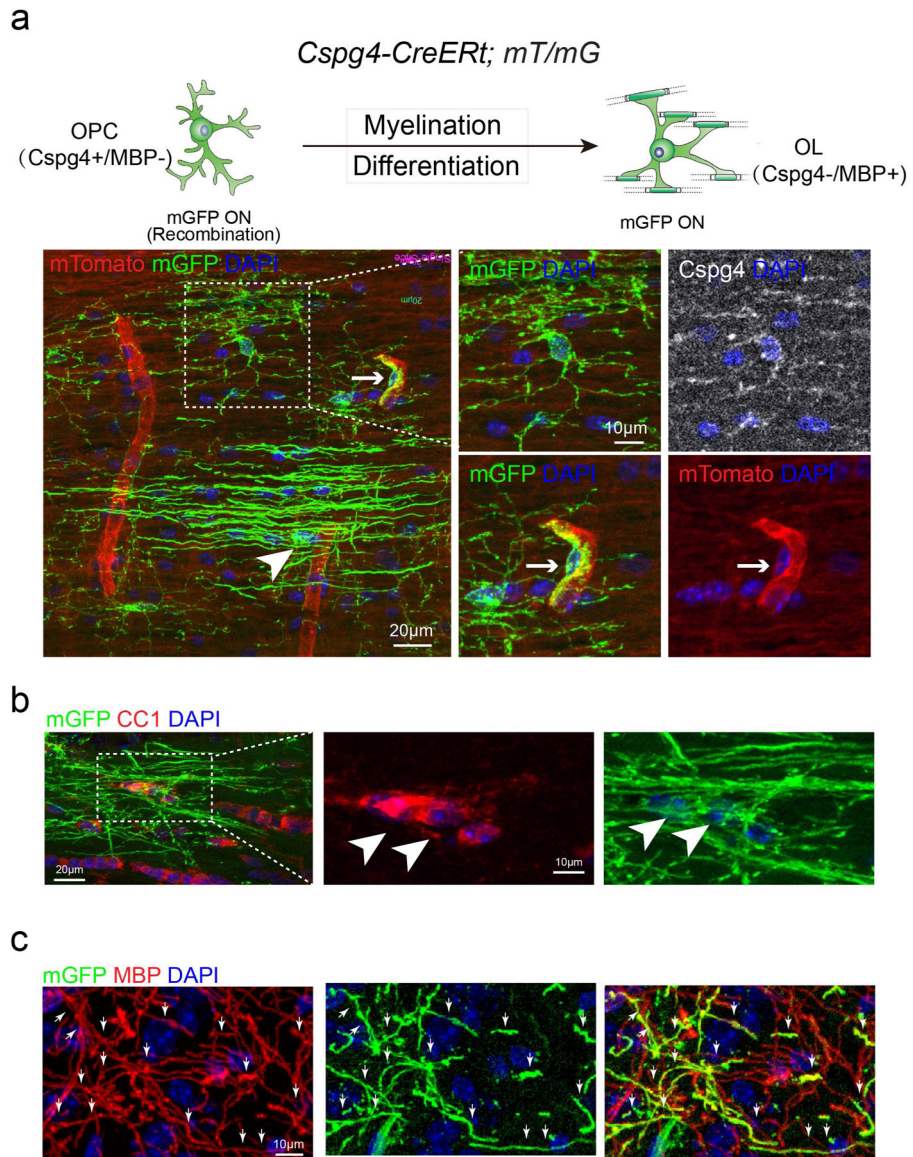
Extended Data Fig. 5 |. expression of mGFP positive cells in the *Cspg4-CreERt; mT/mG* CNS.
a, Schematic illustration showing the mGFP expression pattern in the *Cspg4-CreERt; mT/mG* mice and representative image showing mGFP (green)/Cspg4 (gray) double positive OPCs, putative mGFP positive OLs (arrowhead) and mGFP (green)/mTomato (red) double positive pericytes and blood vessels (right lower panels, arrows), Scale bar: 20 μm; **b**, Immunostaining showing mGFP (green)/CC1 (red) double positive OLs (arrowheads), Scale bar: 20 μm (left panel); 10 μm (middle and right panel); **c**, mGFP (green)/MBP (red) double positive myelin sheaths (arrows), sale bar = 10 μm. These experiments were repeated 3 times independently with similar results.

a

The work flow of separating mGFP+ pericytes, OPCs and OLs

mGFP

mTomato mGFP

mT+/mG+ cells (Pericytes)

Pericytes / Blood vessels

20µm

Cspg4 DAPI mGFP DAPI

mGFP+/Cspg4+ cells (OPCs)

OPCs

50µm

New OLs

mGFP+/Cspg4- cells (New OLs)

Putative new OLs

OPCs New OLs DAPI

0.4mm

b

Cspg4-CreERt; mT/mG + 10 Days

TMF

4 Months + 10 Days

OPCs New OLs DAPI

0.4mm

8 Months + 10 Days

Corpus callosum

13 Months + 10 Days

$p = 0.001$

**

$p = 0.002$

**

Cspg4- mGFP+ area ($\times 10^4 \mu m^2$)

9

6

3

0

4 M 8 M 13 M

$p = 0.980$

$p = 0.984$

Cspg4+ mGFP+ cell# ($\times 10^2 /mm^2$)

2

1

0

4 M 8 M 13 M

Extended Data Fig. 6 |. Segregating mGFP positive pericytes, oPCs and oLs in the *Cspg4-CreERt; mT/mG* brains.

a, The blood vessels (red) /pericytes (green) (mT/mG double positive) are segregated and deducted from the mGFP channel, and the Cspg4 (red)/mGFP (green) double positive OPCs are pseudo-colored in red, Cspg4 immunostaining in *Cspg4-CreERt*; The experiments were repeated 3 times independently with similar results. Scale bar: 20µm (left panels on the top); 50µm (left panels on the bottom); 0.4 mm (right panels); **b**, Schematic diagram displaying the time course of tamoxifen induction and histology in the *Cspg4-CreERt; mT/mG* mice, and representative images of Cspg4 + /mGFP + OPCs (red) and Cspg4-/mGFP + new OLs (green, arrows) in the corpus callosum at 4-, 8- and 13 months, 10 days after induction and quantification of Cspg4 + /mGFP + OPC density and Cspg4-/mGFP + new myelin area, n = 3 biologically independent mice for each group, one-way ANOVA was used followed by post hoc Tukey test (Cspg4-/mGFP+area: $F_{(2,6)} = 97.587$, $p < 0.001$, TUKEY (4 M versus 13 M): $p = 0.001$, TUKEY (8 M versus 13 M): $p = 0.010$; Cspg4+/mGFP+cell: $F_{(2,6)} =$
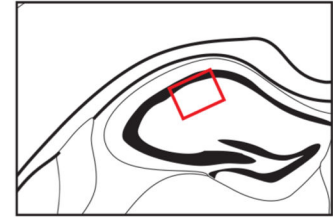
0.066, p = 0.937). Scale bar = 0.4 mm. Points represented individual animals. Error bars represent mean ± s.e.m. **$p < 0.01$.
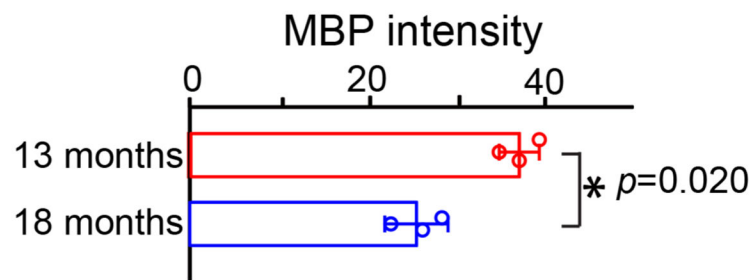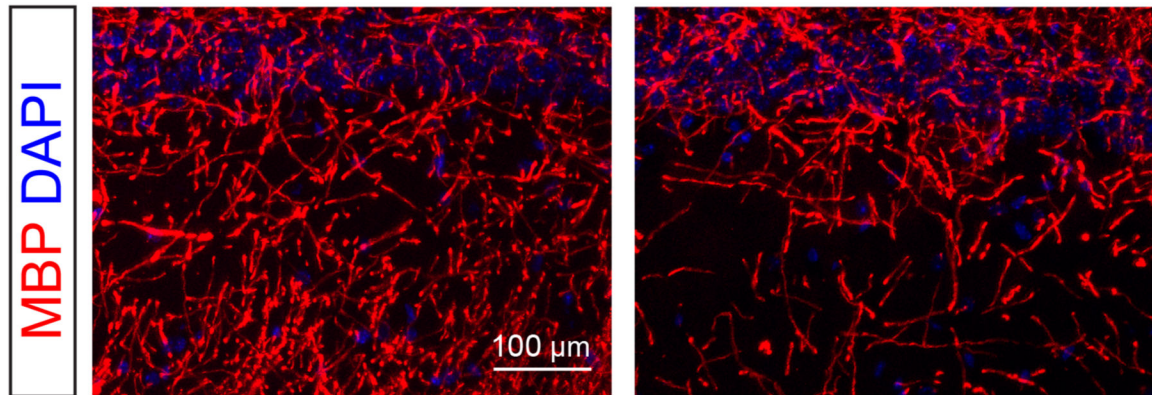
**Extended Data Fig. 7 |. MBP expression in hippocampus at 13- or 18- months of age.**
Representative images and quantification of mean MBP intensity in the CA2 region of the hippocampus. N = 3 biologically independent mice for each group, two-tailed unpaired t test was used ($t_{(4)} = 3.730$, $p = 0.0203$). Scale bar = 100 μm. Points represented individual animals. Error bars represent mean ± s.e.m. $*p < 0.05$.
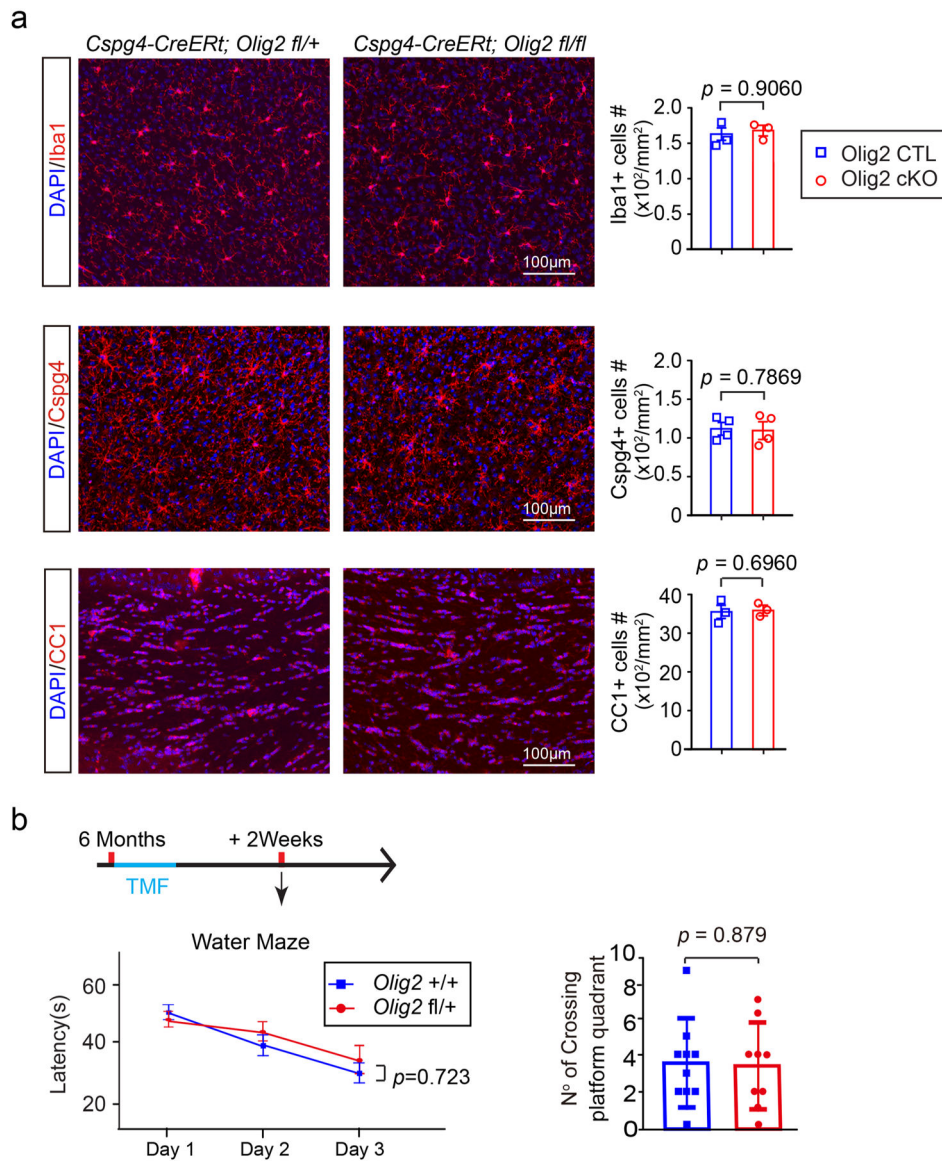
Extended Data Fig. 8 |. oPCs, oLs and microglia in olig2 cKo brains.
a, Representative images and quantification of Iba1, Cspg4, CC1 positive cells in the motor cortex of Olig2 cKO and littermate controls, n = 3 biologically independent mice for the Iba1 and CC1 immunostaining in each group, and n = 4 biologically independent mice for the Cspg4 immunostaining in each group, two-tailed unpaired t test were used (Iba1:$t_{(4)}$ = 0.1257, p = 0.9060; Cspg4:$t_{(6)}$ = 0.2827, p = 0.7869; CC1:$t_{(4)}$ = 0.4201, p = 0.6960); **b**, Schematic diagram displaying the time course of tamoxifen induction and the water maze test. The Morris water maze test showing latency to platform in acquisition phase and numbers of platform crossing of the *Olig2 fl/ +* (n = 9 biologically independent mice) and *Olig2 + / +* (n = 10 biologically independent mice) mice. Two-way repeated ANOVA was used for the latencies to platform ($F_{(1,17)}$ = 0.130, p = 0.723), two-tailed unpaired t test was used for number of platform crossing in the target quadrant ($t_{(17)}$ = 0.03205, p = 0.9748). Scale bar: 100 μm. Points represented individual animals. Error bars represent mean ± s.e.m.
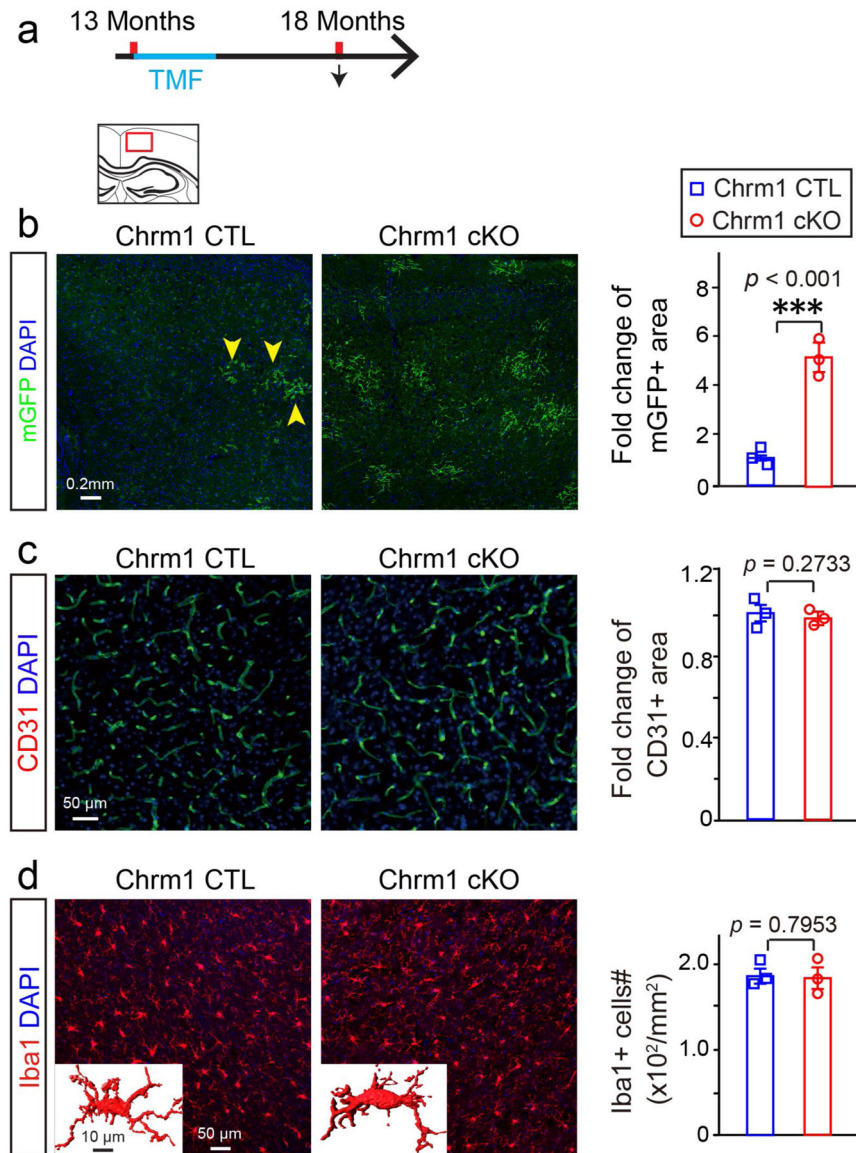
Extended Data Fig. 9 |. Chrm1 deletion in oPCs does not affect blood vessel density and microglia activation.

a, Schematic diagram displaying the time course of tamoxifen induction and histology; **b**, Representative images and quantification of mGFP positive myelin (yellow arrowheads) in the cortex of Chrm1 cKO mice and age-matched wildtypes, scale bar = 0.2 mm; **c**, Representative images and quantification of CD31 positive area in the cortex of Chrm1 cKO mice and age-matched wildtypes, Scale bar = 50μm; **d**, Representative images and quantification of Iba1 positive microglia in the cortex of Chrm1 cKO mice and age-matched wildtypes, Scale bar = 50 μm, n = 3 biologically independent mice for each group for all experiments, two-tailed unpaired t test were used for each group in all experiments (mGFP:$t_{(4)}$ = 11.37, $p < 0.001$; CD31:$t_{(4)}$ = 1.269, p = 0.2733; Iba1:$t_{(4)}$ = 0.2773, p = 0.7953); Inserted images showing 3D Iba1 positive cells, scale bar = 10 μm. Points represented individual animals. Error bars represent mean ± s.e.m. ***$p < 0.001$.

Acknowledgements

References

1. Gazzaley A, Cooney JW, Rissman J & D'Esposito M Top-down suppression deficit underlies working memory impairment in normal aging. Nat. Neurosci 8, 1298–1300 (2005). [PubMed: 16158065]

2. Garde E et al. Relation between age-related decline in intelligence and cerebral white-matter hyperintensities in healthy octogenarians: a longitudinal study. Lancet 356, 628–634 (2000). [PubMed: 10968435]

3. Hughes EG & Orthmann-Murphy JL Myelin remodeling through experience-dependent oligodendrogenesis in the adult somatosensory cortex. Nat. Neurosci 21, 696–706 (2018). [PubMed: 29556025]

4. Young KM et al. Oligodendrocyte dynamics in the healthy adult CNS: evidence for myelin remodeling. Neuron 77, 873–885 (2013). [PubMed: 23473318]

5. Hill RA, Li AM & Grutzendler J Lifelong cortical myelin plasticity and age-related degeneration in the live mammalian brain. Nat. Neurosci 21, 683–695 (2018). [PubMed: 29556031]

6. Lasiene J et al. Age-related myelin dynamics revealed by increased oligodendrogenesis and short internodes. Aging Cell 8, 201–213 (2009). [PubMed: 19338498]

7. McKenzie IA et al. Motor skill learning requires active central myelination. Science 346, 318–322 (2014). [PubMed: 25324381]

8. Zatorre RJ, Fields RD & Johansen-Berg H Plasticity in gray and white: neuroimaging changes in brain structure during learning. Nat. Neurosci 15, 528–536 (2012). [PubMed: 22426254]

9. Hughes EG, Kang SH, Fukaya M & Bergles DE Oligodendrocyte progenitors balance growth with self-repulsion to achieve homeostasis in the adult brain. Nat. Neurosci 16, 668–676 (2013). [PubMed: 23624515]

10. Kang SH et al. NG2+ CNS glial progenitors remain committed to the oligodendrocyte lineage in postnatal life and following neurodegeneration. Neuron 68, 668–681 (2010). [PubMed: 21092857]

11. Wang F et al. Enhancing oligodendrocyte myelination rescues synaptic loss and improves functional recovery after chronic hypoxia. Neuron 99, 689–701e5 (2018). [PubMed: 30078577]

12. Mei F et al. Accelerated remyelination during inflammatory demyelination prevents axonal loss and improves functional recovery. eLife 5, 1–21 (2016).

13. Mei F et al. Stage-specific deletion of Olig2 conveys opposing functions on differentiation and maturation of oligodendrocytes. J. Neurosci 33, 8454–8462 (2013). [PubMed: 23658182]

14. Safaiyan S et al. Age-related myelin degradation burdens the clearance function of microglia during aging. Nat. Neurosci 19, 995–998 (2016). [PubMed: 27294511]

15. Cantuti-Castelvetri L & Fitzner D Defective cholesterol clearance limits remyelination in the aged central nervous system. Science 359, 684–688 (2018). [PubMed: 29301957]

16. Shen S et al. Age-dependent epigenetic control of differentiation inhibitors is critical for remyelination efficiency. Nat. Neurosci 11, 1024–1034 (2008). [PubMed: 19160500]

17. Morrison JH & Baxter MG The ageing cortical synapse: hallmarks and implications for cognitive decline. Nat. Rev. Neurosci 13, 240–250 (2012). [PubMed: 22395804]

18. Mei F et al. Micropillar arrays as a high-throughput screening platform for therapeutics in multiple sclerosis. Nat. Med 20, 954–960 (2014). [PubMed: 24997607]

19. Ruckh JM et al. Rejuvenation of regeneration in the aging central nervous system. Cell Stem Cell 10, 96–103 (2012). [PubMed: 22226359]

20. Nave KA Myelination and the trophic support of long axons. Nat. Rev. Neurosci 11, 275–283 (2010). [PubMed: 20216548]

21. Vorhees CV & Williams MT Morris water maze: procedures for assessing spatial and related forms of learning and memory. Nat. Protoc 1, 848–858 (2006). [PubMed: 17406317]
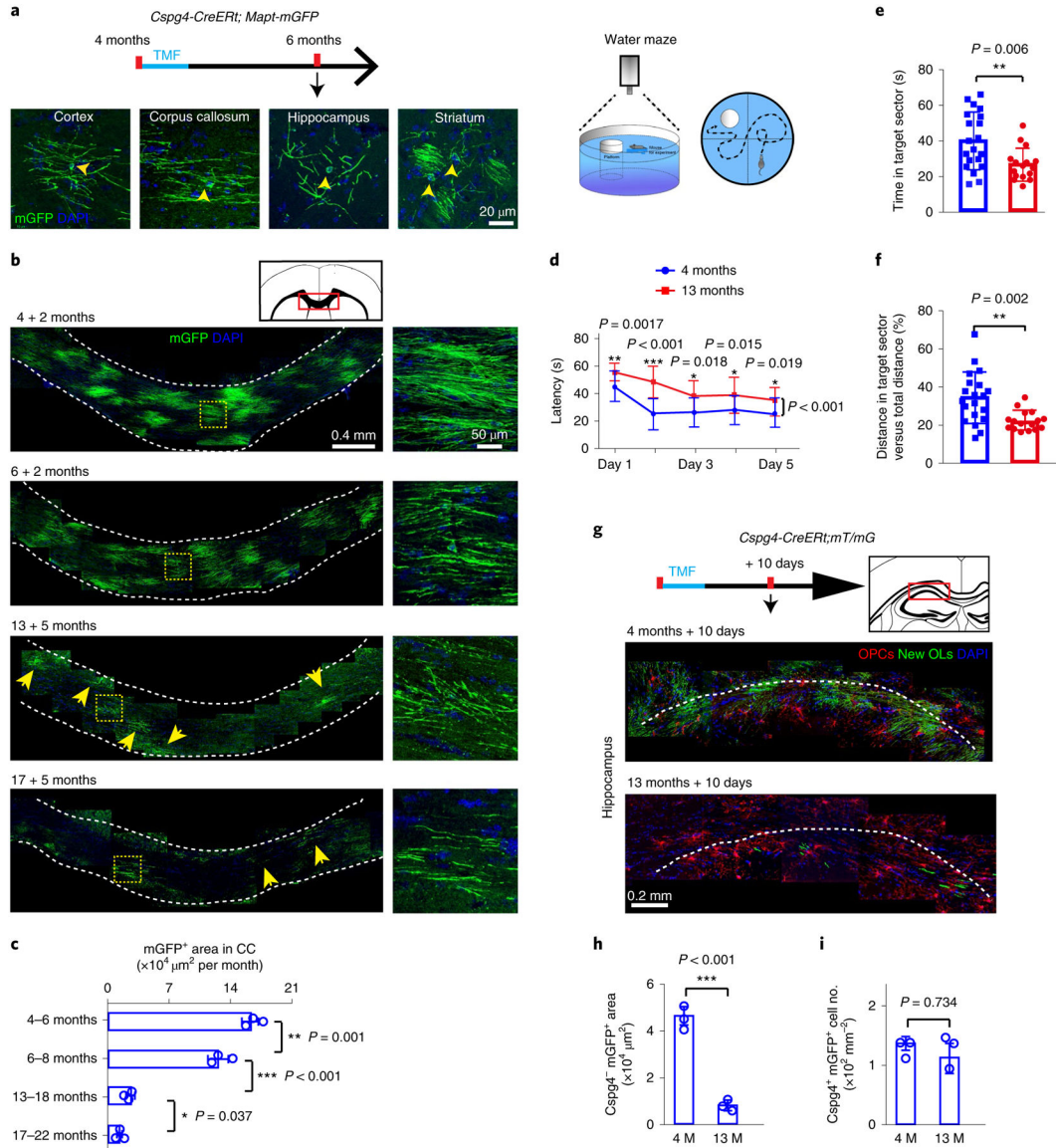
Fig. 1 |. age-related myelin renewal and memory deficits in aging mice.
a, Schematic diagram displaying the time course of tamoxifen induction and histology in the *Cspg4-CreERt;Mapt-mGFP* mice, and representative images showing mGFP-positive oligodendrocytes (yellow arrowheads) and associated myelin sheaths in cortex, corpus callosum, hippocampus and striatum, 2 months after recombination at 4 months (4 + 2 months); scale bar, 20 μm. **b**, mGFP-positive oligodendrocytes and myelin sheaths (yellow arrows) in the corpus callosum of 4 + 2-, 6 + 2-, 13 + 5- and 17 + 5-month-old mice. Enlarged images (right panels) correspond to the dotted boxes in the left panels. These experiments were repeated three times independently with similar results. Scale bars, 0.4 mm (left panels); 50 μm (right panels). **c**, Quantification of mGFP-positive area in corpus callosum; $n = 3$ biologically independent mice for each group; one-way ANOVA was used followed by post hoc Tukey test (mGFP positive area: $F_{(2,6)} = 424.949$, $P < 0.001$; Tukey (4 + 2 months versus 6 + 2 M): $P = 0.001$; Tukey (6 + 2 months versus 13 + 5 months): $P <$

0.001; Tukey (13 + 5 months versus 17 + 5 months): $P = 0.037$). **d–f**, The Morris water maze test reveals the latency to platform in the acquisition phase (**d**), and time (**e**) and distance (**f**) spent in the target quadrant in the 4-month-old ($n = 20$ biologically independent mice) and 13-month-old ($n = 16$ biologically independent mice) mice. Two-way repeated ANOVA was used for the latencies to platform (**d**): $F_{(1,34)} = 44.928$, $P < 0.001$; day 1, unpaired t-test ($P = 0.0017$); day 2, unpaired t-test ($P < 0.001$); day 3, unpaired t-test ($P = 0.018$); day 4, unpaired t-test ($P = 0.015$); day 5, unpaired t-test ($P = 0.019$); two-sided unpaired Mann–Whitney tests were used for time spent in target sector (**e**): $U(34) = 76$, $P = 0.0065$ and distance traveled in target sector vs total distance (**f**): $U(34) = 65$, $P = 0.0019$. **g–i**, Schematic diagram displaying the time course of tamoxifen induction and histology in the *Cspg4-CreERt;mT/mG* mice, along with representative images of Cspg4$^+$mGFP$^+$ OPC (red) density and Cspg4$^-$mGFP$^+$ new myelin (green) area in the hippocampus 10 d after tamoxifen treatment at 4 and 13 months (**g**); quantification of Cspg4$^-$mGFP$^+$ new myelin area (**h**) and Cspg4$^+$mGFP$^+$ OPC density (**i**); $n = 3$ biologically independent mice for each group, two-tailed unpaired t-tests were used (NG2$^-$mGFP$^+$ area, **h**: $t_{(4)} = 15.11$, $P < 0.001$; NG2$^+$mGFP$^+$ cells, **i**: $t_{(4)} = 0.3621$, $P = 0.7335$); scale bar, 20 μm. Points represent individual animals. Error bars represent mean ± s.e.m. $*P < 0.05$, $**P < 0.01$, $***P < 0.001$. CC, corpus callosum; OL, oligodendrocyte; TMF, tamoxifen.
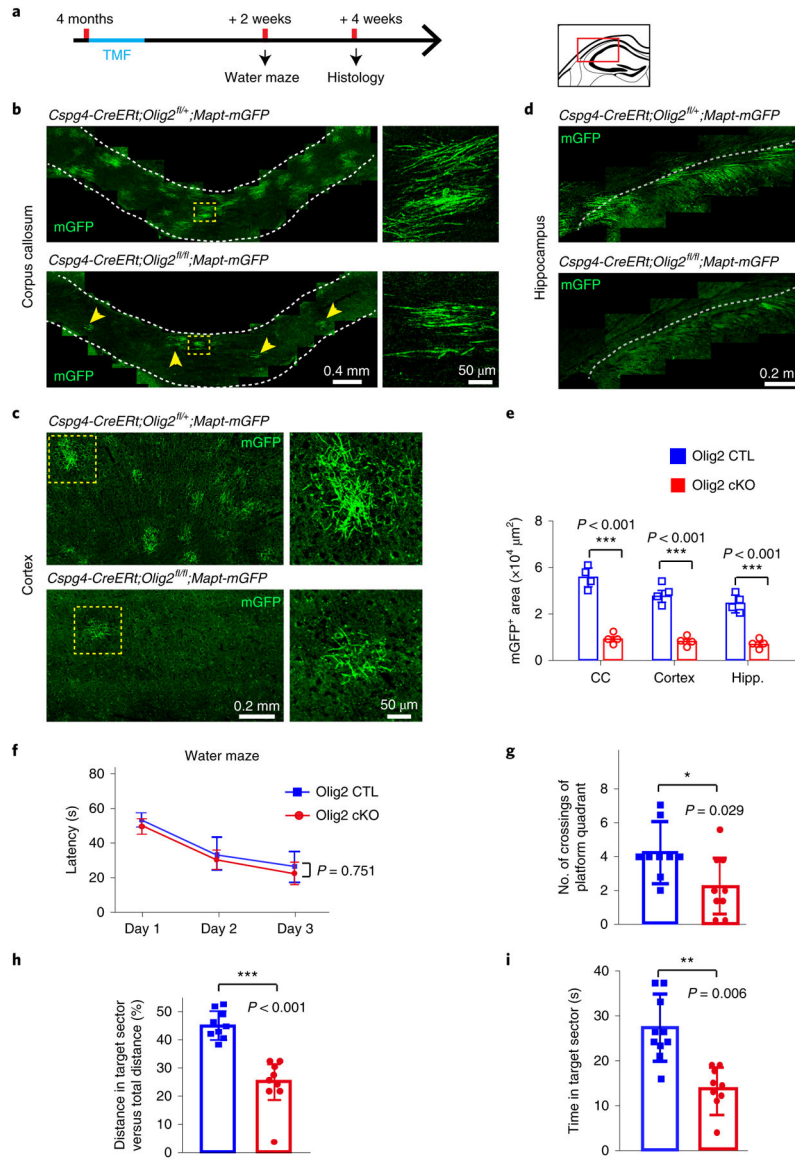
Fig. 2 |. *Olig2* deletion in oPCs inhibits myelination and impairs spatial memory in 4-month-old mice.

a, Schematic illustration displaying the time course of tamoxifen induction, histology and water maze test. **b–d**, Representative images showing mGFP[+] myelin (arrows) in the corpus callosum (**b**), cortex (**c**) and hippocampus (**d**) of Olig2 cKO brains and littermate controls. Right panels of enlarged images correspond to dotted boxes of left panels (**b** and **c**). These experiments were repeated four times independently with similar results. Scale bars, 0.4 mm (left panels of **b**), 50 μm (right panels of **b**), 0.2 mm (left panels of **c**), 50 μm (right panels of **c**) and 0.2 mm (**d**). **e**, Quantification of mGFP[+] area in Olig2 cKO brains and littermate controls; $n = 4$ biologically independent mice for each group, two-tailed unpaired t-tests were used; corpus callosum: $t_{(6)} = 20.28$, $P < 0.001$; cortex: $t_{(6)} = 13.94$, $P < 0.001$; hippocampus (Hipp.): $t_{(6)} = 13.34$, $P < 0.001$). **f–i**, The Morris water maze test showing latency to platform in acquisition phase (**f**), number of platform crossings (**g**), and distance (**h**) and time (**i**) spent in the target quadrant in the Olig2 cKO mice and littermate controls; n

= 9 biologically independent mice for each group. Two-way repeated ANOVA was used to analyze the latencies to platform ($F_{(1,16)} = 0.104$, $P = 0.751$); two-tailed unpaired t-tests were used for number of platform crossings (**g**: $t_{(16)} = 2.339$, $P = 0.029$), distance (**h**: $t_{(16)} = 4.071$, $P < 0.001$) and time (**i**: $t_{(16)} = 3.193$, $P = 0.006$) spent in the target quadrant for each group. Points represent individual animals. Error bars represent mean ± s.e.m. *$P < 0.05$, **$P < 0.01$, ***$P < 0.001$. CTL, control.
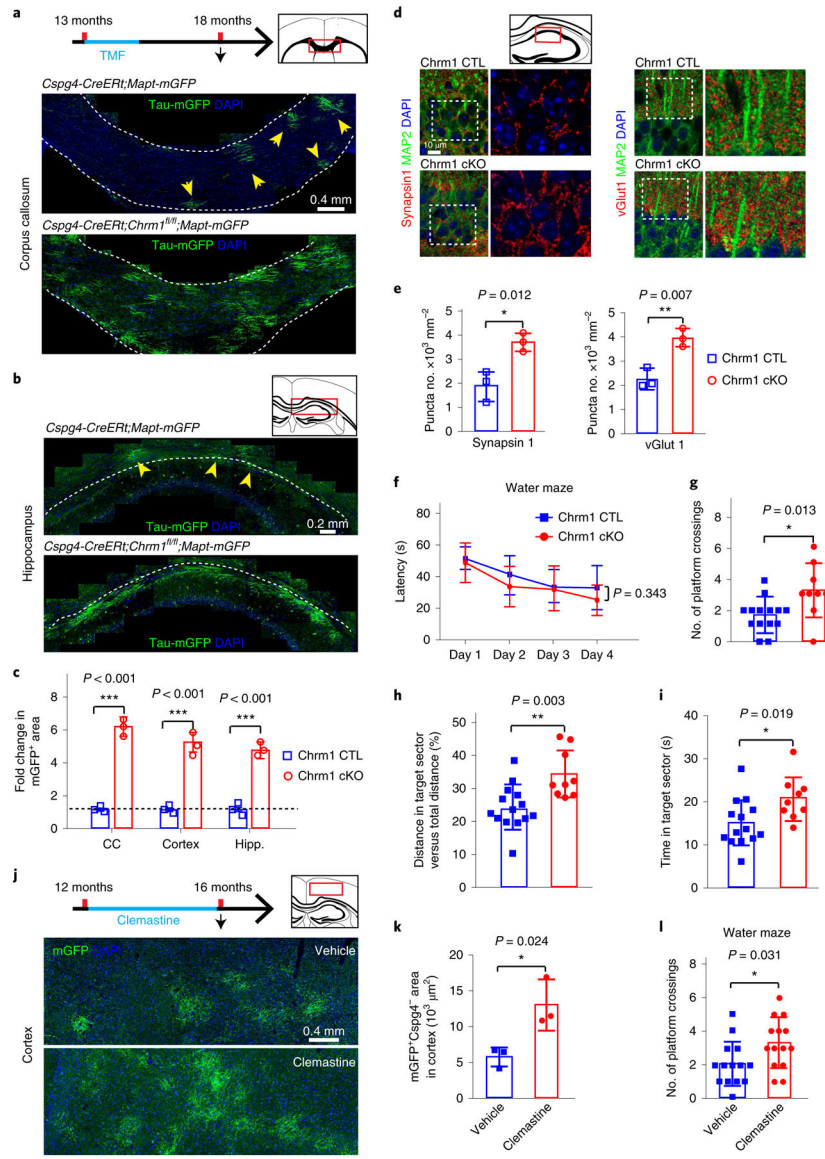
Fig. 3 |. *Chrm1* deletion in oPCs or clemastine treatment enhances myelination and reverses the spatial memory deficit in aging mice.

a,**b**, Schematic diagram displaying the time course of tamoxifen induction, histology and water maze test, and representative images showing mGFP[+] myelin (yellow arrowheads) in the corpus callosum (**a**) and hippocampus (**b**) of Chrm1 cKO mice and age-matched wild types. These experiments were repeated three times independently with similar results. Scale bars, **a**, 0.4 mm; **b**, 0.2 mm. **c**, Quantification of fold change of mGFP[+] areas in the corpus callosum and hippocampus; $n = 3$ biologically independent mice for each group, two-tailed unpaired t-tests were used (CC: $t_{(4)} = 23.52$, $P < 0.001$; hippocampus: $t_{(4)} = 14.11$, $P < 0.001$). **d**,**e**, Representative images (**d**) and quantification (**e**) of synapsin1[+] and vGlut1[+] synaptic puncta (red) and MAP2 (green) neurons in the CA1 region by immunostaining in the Chrm1 cKO and wild types; enlarged images (right panels) correspond to dotted boxes in left panels. These experiments were repeated three times independently with similar results; $n = 3$ biologically independent mice for each group, two-tailed unpaired t-tests were used for

quantification of synapsin1 ($t_{(4)}$ = 4.343, P = 0.012) and vGlut1 ($t_{(4)}$ = 5.181, P = 0.0066); scale bar, 10 μm. **f–i**, The Morris water maze test revealing latency to platform in acquisition phase (**f**), numbers of platform crossings (**g**), distance (**h**) and time (**i**) spent in the target quadrant in the Chrm1 cKO mice (n = 9 biologically independent mice) and wild-type controls (n = 14 biologically independent mice). Two-way repeated ANOVA was used for the latencies to platform (**f**: $F_{(1,21)}$ = 0.941, P = 0.343); two-tailed unpaired t-tests were used for number of platform crossings (**g**: $t_{(21)}$ = 2.721, P = 0.0128), distance (**h**: $t_{(21)}$ = 3.351, P = 0.003) and time (**i**: $t_{(21)}$ = 2.528, P = 0.0195) spent in the target quadrant. **j**, Schematic diagram displaying the time course of clemastine treatment, histology and water maze test, and representative images showing Cspg4⁻mGFP⁺ myelin in the cortex of *Cspg4-CreERt;mT/mG* brains; scale bar, 0.4 mm. **k**, Quantification of Cspg4⁻mGFP⁺ myelin; n = 3 biologically independent mice for each group, two-tailed unpaired t-test was used ($t_{(4)}$ = 3.521, P = 0.0244). **l**, Number of platform crossings of the mice treated with clemastine or vehicle by Morris water maze test; n = 14 biologically independent mice for each group, two-tailed unpaired t-test was used ($t_{(26)}$ = 2.276. P = 0.0313). Points represent individual animals. Error bars represent mean ± s.e.m. *P < 0.05, **P < 0.01, ***P < 0.001.